Mooring forces in a floating point-absorbing WEC system – a comparison between full-scale measurements and numerical simulations

(article starts on next page)

Mooring forces in a floating point-absorbing WEC system – a comparison between full-scale measurements and numerical simulations

Jonas W. Ringsberg [a], Shun-Han Yang[a], Xiao Lang[a], Erland Johnson[b] and Jonas Kamf[c]

[a]Department of Mechanics and Maritime Sciences, Chalmers University of Technology, Gothenburg, Sweden; [b]RISE Research Institutes of Sweden, Borås, Sweden; [c]W4P Waves4Power AB, Gothenburg, Sweden

ABSTRACT

The study presents an investigation of Waves4Power's WaveEL 3.0 wave energy converter (WEC). It was used as a reference for full-scale measurements of the mooring forces and buoy motions in a measurement campaign 2017 at an installation location off the coast of Runde in Norway. A numerical simulation model of the installation was developed in the DNV GL software SESAM. Unfortunately, the sea state conditions were not measured during the measurement campaign. Hence, a methodology was developed that used the recorded motion data to compute the sea state conditions at the test site. The simulated WEC motions based on the computed sea states agreed very well with the measured WEC motions. The measured and simulated mooring forces were compared under various environmental conditions. 3-hour sea state realizations are typically preferred in numerical simulations. However, influences from the tide at the test site showed that sea states were normally stationary for only 1–2 h. The measured and simulated average mooring forces agreed very well during 1-hour periods, whereas the simulations overestimated the mooring forces in 3-hour periods because of the tide.

1. Introduction

Floating point-absorbing wave energy converters (WECs) can extract energy from waves. Several companies have proposed concepts for such devices, but none have reached the commercial market. Research and product development are ongoing, wherein simulation models must be validated against laboratory ocean basin tests and field tests and the proposed concepts must be transitioned from prototype to full scale.

Waves4Power deployed a full-scale prototype of their WEC system, WaveEL 3.0, at a test site off the coast of Runde in Norway (Waves4Power 2019). Their WEC system is instrumented with several sensors and equipment that record several factors, such as the WEC's motions and position, axial forces in the mooring lines, the power performance of the WEC and the responses of the power cable that goes from the WEC to a power-collecting hub. This WEC system was part of a full-scale measurement campaign lasting from June to November 2017. Yang (2018) and Yang et al. (2018a) developed a numerical simulation model of the WaveEL 3.0 system installed in Runde. Their simulation procedure has been validated against model tests performed in a laboratory ocean basin (see Yang et al. (2018b) regarding WEC motions and Yang et al. (2019) regarding mooring forces). This model was used in the current study to simulate the real environmental conditions at the Runde test site and to compare the simulation results against full-scale measurements.

The availability of results from measurements made on full-scale WEC installations is scarce. One purpose of this study is to share research results and experiences that may stimulate the advancement of technologies and models for floating point-absorbing WEC systems. A second purpose of the study was to investigate the prediction capacity of the numerical model by comparing the numerical simulation results with full-scale measurements. This report is a continuation of the study reported by Lang et al. (2018). However, in the current study, additional measurement data are presented and discussed in detail with regard to the model and measurement uncertainties.

The following sections present how the recorded data from different sensors were analysed and compared to the simulation results. The following sections also present how the lack of measurement data of the sea state conditions at the test site and the deviations and sources of uncertainties in the full-scale measurements have been identified and mitigated in the numerical simulations. Section 2 presents the full-scale installation and the first method developed in this study for the coordination of various measurement data. Section 3 presents the validated numerical model used to calculate the hydrodynamic and structural responses of WEC systems. Section 3 also presents the second method developed in this study, which uses data from the measurements of the WEC's motions to estimate the environmental loads imparted on the WEC, and the stationary sea states that should be used in the numerical simulations to achieve the same WEC motion responses. Section 4 presents the comparison of results from measurement and
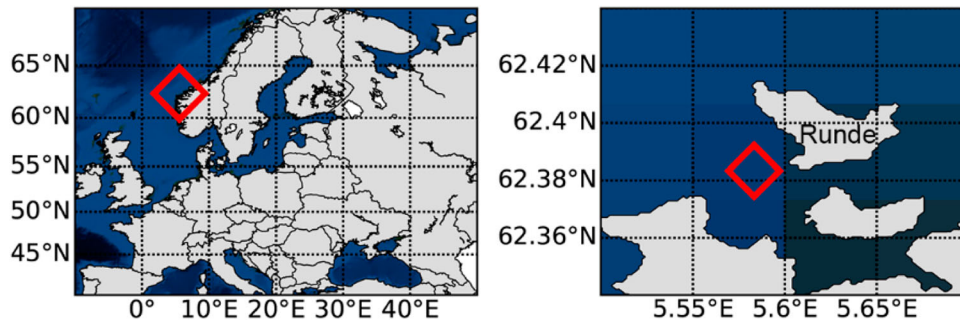
Figure 1. (Left) Runde, Norway, and (right) WEC WaveEL 3.0 location.

numerical simulations. Discussions on the uncertainties of the study are presented in Section 5, and the conclusion of the study is presented in Section 6.

2. WaveEL 3.0 installation

2.1. Descriptions of the test site and installation

WaveEL 3.0 is the name of Waves4Power's installed WEC system on the test site in Runde, Norway. This WEC was in full operation for a measurement campaign from June to November 2017. The location and position of the WEC are shown in Figure 1.

An illustration of the WEC system installation is shown in Figure 2. WaveEL 3.0 is a floating point-absorber WEC which extracts energy from waves from heave motions. WaveEL 3.0 has an elastic mooring system that consists of three mooring legs, and each mooring leg has two segments with a submerged floater connecting the two segments. Gravity anchors are used to fix the WEC to the seabed. A dynamic power cable transfers the power from the WEC to a hub.

WaveEL 3.0 has a taut mooring system with polyester mooring lines designed for 25 years of operation. Although polyester is widely used for deep-water moorings, its long-term durability in a marine environment requires additional research and physical testing (Banfield et al. 1999). The gravity anchors are not placed at the same water depth due to a small inclination of the seabed, and hence, the lengths of the mooring lines vary by a few metres.

2.2. Instrumentation and full-scale measurements: mooring forces and buoy motions

The axial forces in the three mooring lines were measured during two periods in 2017: June 1 to July 3 and October 4

to November 22, where the latter was an additional measurement period compared to the measurement period presented in Lang et al. (2018) A Dacell CLM-T50 pressure sensor measured the compression between the moving sledge with a mooring bollard structure and the fixed structure welded to the buoy's hull (see Figure 3).

During the post-processing of the measurement data, a malfunction was detected in the pressure sensor of one mooring line (Mooring 3 in Figure 7). Hence, measurement data for only two of the mooring lines were used in this study. The axial forces in these mooring lines were sampled at 10 Hz from June 1–17 and thereafter at 60 Hz throughout the remaining measurement period; the measurement accuracy is 10 N.

The WEC's motions were measured from 15:00:00 on June 13 to 22:00:00 on June 19, which overlapped a portion of the first measurement period. The WEC was instrumented with a number of different sensors that measured its translations and rotations. The positions of the WEC were tracked by a global navigation satellite system (GNSS) sensor (a JAVAD receiver and a LEICA antenna). The rotations were measured by a vertical gyro (VG) sensor (MEMSIC VG-350). All motions were measured at the sampling frequency of 2 Hz, and the measurement accuracy is 3 cm for the translational motion (GNSS sensor) and 0.75° for the rotational motions (VG sensor). The pitch and roll measurements were highly accurate, but the yaw angle had lower accuracy because the sensor could only measure short-term movements around the vertical axis at the sensor installation position. These sensors were mounted on the weather deck on the top of the WEC buoy (see Figure 4).
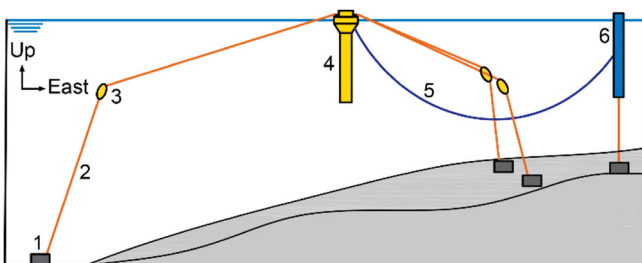

Figure 2. Illustration of the WaveEL 3.0 installation in Runde: (1) gravity anchor, (2) mooring line segment, (3) floater, (4) WEC, (5) power cable, and (6) hub.
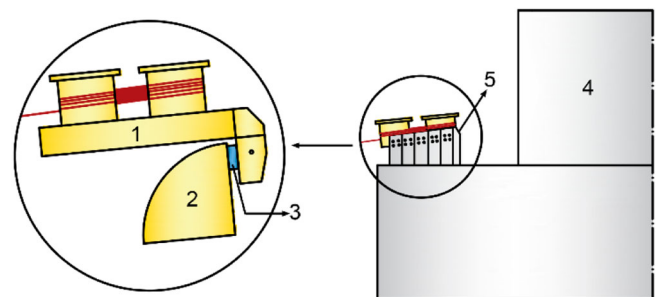

Figure 3. Illustration of the pressure sensor installation: (1) bollard structure, (2) fixed structure, (3) pressure sensor, (4) WEC buoy, and (5) moving sledge.
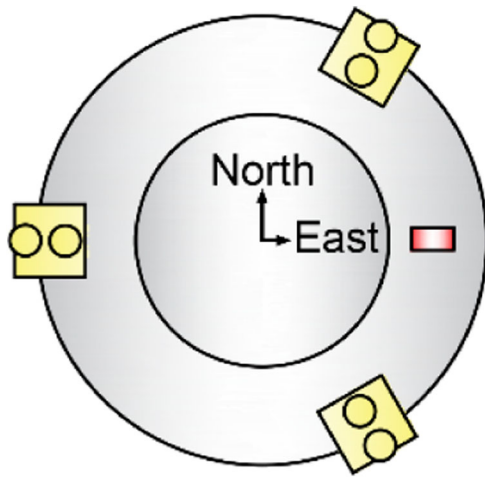
Figure 4. Top view of the WEC buoy, where the red box shows the location of the sensors used to measure the translations and rotations of the WEC.

2.2.1. Transformation of the WEC's motion

The data from the different sensors were not collected in a systematic procedure and required post-processing and additional calculations to describe the WEC's motions in six degrees of freedom (DOFs). As noted in Section 2.2, the measurements by the VG sensor for the long-term yaw angle was less reliable; a correction of the long-term motion measurement in the yaw direction is needed. The long-term measurement of WEC motion was used to reconstruct the WEC's initial position and a consistent coordinate system among the various sensors. Although there was no 'reliable' value of the measured yaw angle, the short-term variations could be trusted. These variations were deemed realistic and caused by the waves; the variation in the yaw angle should also be small due to the mooring system design. Thus, a method was developed to estimate the yaw motions, with the long-term response corrected. The original sensor yaw measurements were high-pass filtered, arbitrary drift was removed and high-frequency (short-term) components of the yaw angle were preserved. For each hour of analysis, the azimuth angle within the VG sensor's x-y plane where the combination of roll and pitch gave the largest tilt variations in the z component was recorded. The topocentric azimuth angle in the East-North plane was tracked when the GNSS antenna experienced its largest horizontal motion. The azimuth angles of the largest tilt variation and largest horizontal motions were separated by approximately 63° over the whole measurement period; however, these angles should be approximately in the same physical direction (see Figure 5).

The value seems to fit most of the data, especially for the mid and later analysis periods of the measurement time span. Thus, it was assumed that the VG sensor in the x-y plane can be rotated by 63° relative to the topocentric East-North. Then, the long-term correction component was used to recover the yaw angle. Since the orientation of the VG sensor was known, the WEC buoy centre rotations and translations were computed using the VG sensor Euler angles and the GNSS antenna positions. The sampling frequency of the WEC's motion responses was 10 Hz after the data had been post-processed.
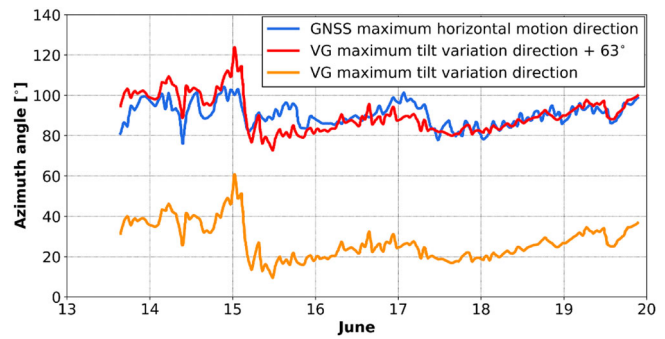

Figure 5. Azimuth angle comparison between the maximum VG sensor tilt variation and the GNSS sensor horizontal motion direction. The data were used to recover the WEC's yaw angle.

3. Simulation model of WaveEL 3.0

3.1. Description of the model

The numerical model of WaveEL 3.0 was developed using the commercial software package DNV GL SESAM (DNV GL 2019) and it is used to simulate the hydrodynamic and structural response of the WEC system. Figure 6 illustrates the entire analysis workflow; it combines the boundary element method to simulate and solve the potential flow theory for the wave-structure interaction and the finite element method to simulate and calculate the motions and structural responses of the mooring lines and power cable. A viscous drag formulation is used for wind and current loads and in the Morison equation. The readers are referred to Yang (2018) and Yang et al. (2016) for the comprehensive description of the objective, limitation, and theoretical formulation of the numerical model and simulation method.

Owing to the mechanical coupling between the WEC and the slender structures (namely, mooring lines and power cable), a time-domain coupled simulation procedure was adopted in this study, performed at Step 3 in Figure 6. The coupled procedure simultaneously solves the equation of motions of the WEC buoy, mooring lines, and power cable using time-domain analysis, and thus the motion and force of the slender structures implicitly influence the instantaneous dynamics of the WEC buoy and vice versa. The coupled simulation model used in the study was developed by Yang et al. (2018a) and adapted to the Runde test site conditions and installation; see Yang (2018) for details. A top view of the system is shown in Figure 7. The motion responses of the WEC were solved in SIMO (SINTEF Ocean 2018b), whereas the hydrodynamic and structural analyses of all components were performed in RIFLEX (SINTEF Ocean 2018a).

3.2. Descriptions of the environmental loads and simulation cases

3.2.1. Load identification

The environmental loads (e.g. wave, wind, and ocean current) on the test site were not included or measured during the measurement campaign. To enable a comparison between the numerical simulations and the full-scale measurement data, a methodology is needed to estimate the environmental loads
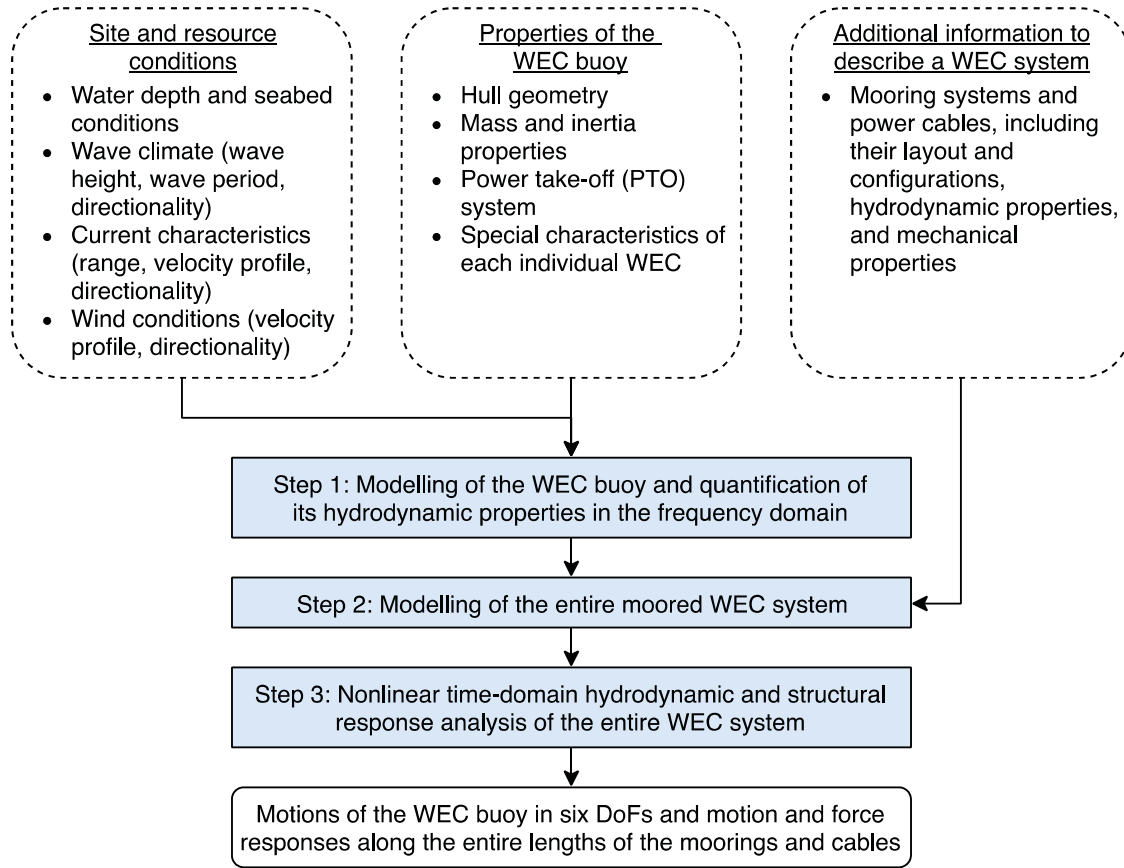
Figure 6. Analysis workflow of the numerical simulation of the WEC system.

imparted on the WEC that caused its motions. An advanced real-time prediction method of ocean waves has been proposed by Kosleck (2014). The method is however not adopted in this study due to the lack of surface elevation snapshots—the input for the prediction method—in the area of the installation site. In the absence of the in-situ data, another method is developed and it is presented in this sub-section.

The first part of the methodology uses the response amplitude operators (RAOs) of the WEC (see the outline of the overall procedure in Figure 8). The RAOs of the WEC were calculated by performing coupled numerical simulations (cf. Figure 6) for the entire WEC system for various sea state conditions.

The heave motion responses were extracted from the numerical simulations and used in a statistical analysis with the WAFO Toolbox (WAFO group 2017). The mean values

of the WEC's heave motion up-crossing height, H_u, and the up-crossing period, T_u, were calculated. A polynomial regression model was developed using the MATLAB Curving Fitting Toolbox (The MathWorks, Inc. 2016) to obtain a regression relation between H_u and T_u and the significant wave height, H_s, and wave peak period, T_p.

Figure 9 presents the wave scatter diagram at the test site, which was used as a basis for the simulations for the regression
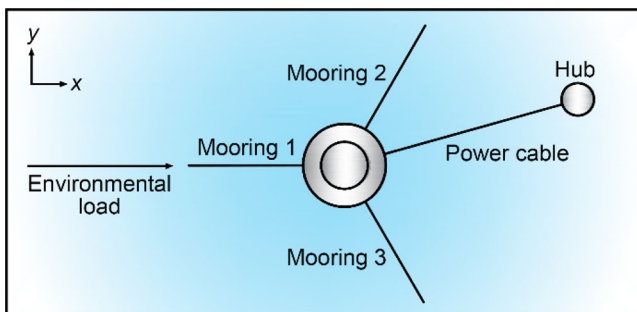

Figure 7. A top view of the WEC system simulation model. The incident environmental load direction is defined as 0° in the figure.
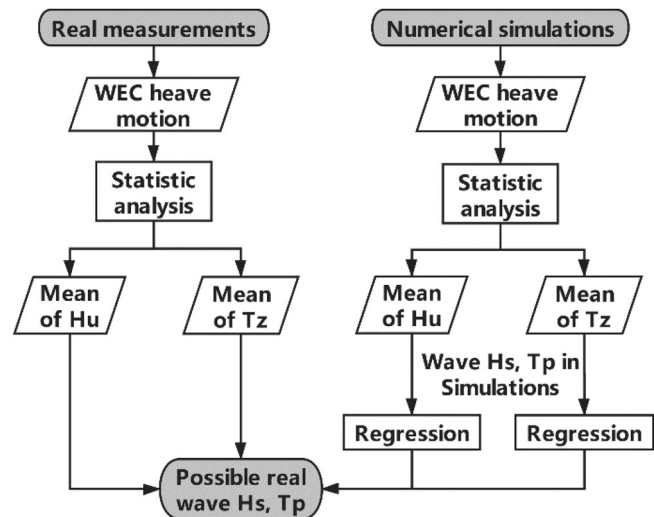

Figure 8. Outline of the wave estimation methodology using WEC buoy heave motions.

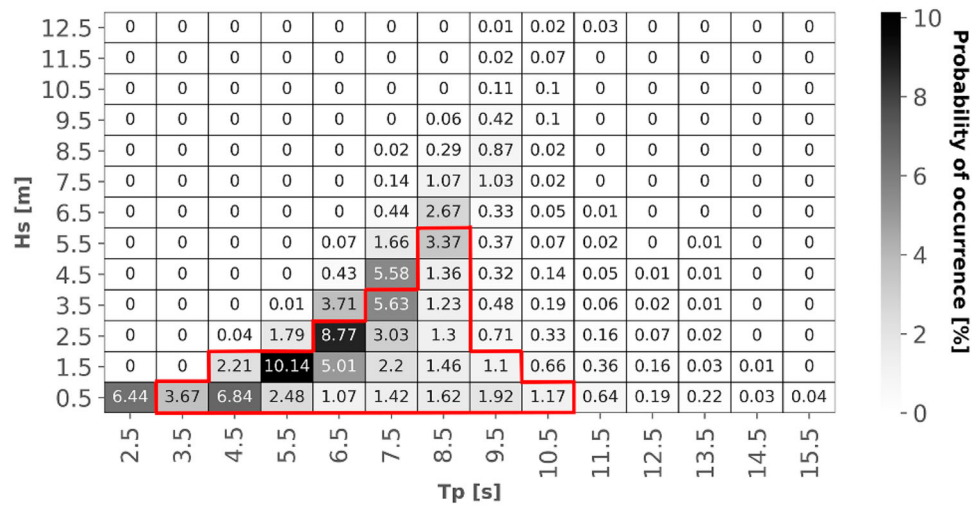| Hs [m] \ Tp [s]	2.5	3.5	4.5	5.5	6.5	7.5	8.5	9.5	10.5	11.5	12.5	13.5	14.5	15.5
12.5	0	0	0	0	0	0	0	0.01	0.02	0.03	0	0	0	0
11.5	0	0	0	0	0	0	0	0.02	0.07	0	0	0	0	0
10.5	0	0	0	0	0	0	0	0.11	0.1	0	0	0	0	0
9.5	0	0	0	0	0	0	0.06	0.42	0.1	0	0	0	0	0
8.5	0	0	0	0	0	0.02	0.29	0.87	0.02	0	0	0	0	0
7.5	0	0	0	0	0	0.14	1.07	1.03	0.02	0	0	0	0	0
6.5	0	0	0	0	0	0.44	2.67	0.33	0.05	0.01	0	0	0	0
5.5	0	0	0	0	0.07	1.66	3.37	0.37	0.07	0.02	0	0.01	0	0
4.5	0	0	0	0	0.43	5.58	1.36	0.32	0.14	0.05	0.01	0.01	0	0
3.5	0	0	0	0.01	3.71	5.63	1.23	0.48	0.19	0.06	0.02	0.01	0	0
2.5	0	0	0.04	1.79	8.77	3.03	1.3	0.71	0.33	0.16	0.07	0.02	0	0
1.5	0	0	2.21	10.14	5.01	2.2	1.46	1.1	0.66	0.36	0.16	0.03	0.01	0
0.5	6.44	3.67	6.84	2.48	1.07	1.42	1.62	1.92	1.17	0.64	0.19	0.22	0.03	0.04

Figure 9. Representative wave scatter diagram of the Runde test site. The value in each cell is the probability of occurrence (%), where the sum of all the cells yields a probability of 1. The cases that were simulated are the cells inside the red frame where linear wave theory applies.

analysis. Only wave conditions within the range of linear theory with a probability of occurrence large than 1% were simulated. The motivation for including solely the linear wave cases was due to the calm-measured WEC motions together with the calm seas predicted by the Runde Environmental Centre (2018). Each wave condition was defined by H_s, T_p, and the wave loading direction (θ) and followed the JONSWAP spectrum. A sea state is described in terms of its duration of stationarity, usually taken to be 3 h (DNV GL 2017). Hence, the simulation time was set to 3 h (10,800 s) for all of the simulations.

The results from the numerical simulations are presented as fitted surfaces in Figure 10. The goodness of fit was assessed by adjusted R-square, which were 0.998 for H_u and 0.9996 for T_u. This shows that the method can predict H_s and T_p if H_u and T_u of the heave motion have been calculated from the measurement data.

The mean value and standard deviation of the WEC's motions were analysed to study the stationarity of the sea states. Figure 11 shows an example of how the WEC's position varied in the horizontal plane (position in East and North) together with its heave motion (vertical position). In the analyses of the measurement data, motions that were relatively stable during a 3-hour time span were sought because they define a stationary sea state. Figure 11 shows a grey time span where the sea state is relatively stationary; the WEC motion during this 3-hour period was then used to calculate the sea state to which the WEC system is subjected. Note, however, from Figure 11, that the WEC's motion in the heave direction exhibits a recurrent shift in its mean position—an observation that could potentially undermine the criterion of 3-hour stationary sea states. The cause of this observation was attributed to the presence of near-shore tide at the test site, and its impacts on the result uncertainties is discussed in Section 5.

Apart from a short duration when the WEC motions were available for load identification, the majority of the measurements were for the mooring forces; therefore, an alternative methodology to identify loadings was needed. In this study, the forecast data provided by the EU Copernicus Marine Environment Monitoring Service (CMEMS 2017) were adopted. The CMEMS data are based on the forecast analysis
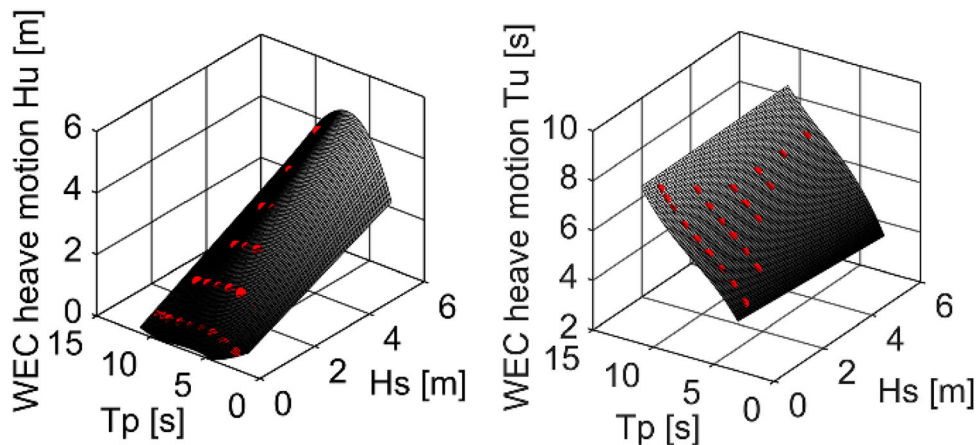
Figure 10. Fitted surfaces from the numerical simulations that relate the mean value of the WEC heave motion H_u (left) and T_u (right) to the significant wave height, H_s, and wave peak period, T_p.
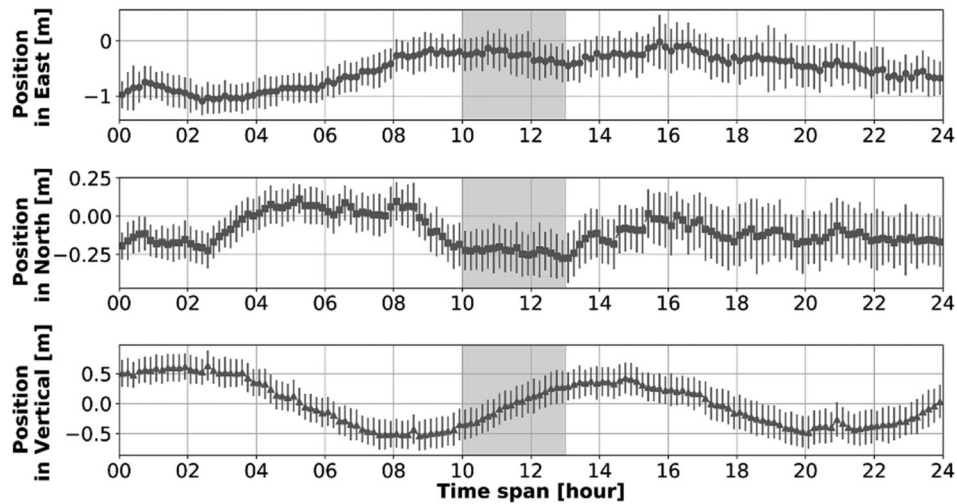
Figure 11. Measurement results from June 16, 2017, which show the WEC's horizontal and vertical motions. The mean values and standard deviations are presented with a resolution of 10 min. The marked grey time span shows an example of a stationary sea state.

using the wave model WAVEWATCH III (CMEMS 2017), which provides several ocean data variables, such as H_s, T_p, and θ, at hourly intervals for the North-East Atlantic region. Although this forecast analysis was originally developed to simulate the open water approximately 20 km or more from the coastline due to the coarse grid resolution of 7 km (Saulter 2017), the simulated region covers the test site location. Hence, the CMEMS data can be used to estimate the sea states at an acceptable level of confidence. In this study, the sea state conditions at the closest available grid point to the installation site (2.3 km away) were extracted from the CMEMS data. Using the same principle used to identify the stationary WEC motions, durations with stationary sea states were identified from the CMEMS data, and the corresponding data were used to define the loading conditions for the numerical simulations.

3.2.2. Simulation cases
Table 1 presents the 7 time periods of stationary sea states identified from the measured WEC motions, which were used to define the wave loads in each numerical simulation. The

corresponding predictions for these 7 periods using the CMEMS data are also shown in the table for comparison. Reasonable correlations were found with regard to H_s and T_p but not for θ; the deviation in θ will be treated as one uncertainty source and is discussed in Section 5. For the remaining measurement period without WEC motion measurements, 23 stationary periods were identified. Figure 12 presents all the hourly predicted sea state conditions from the CMEMS data for these periods; the sea state of each of these periods in the numerical simulations was defined by taking the average of H_s, T_p, and θ for every three consecutive hours.

The sea states presented in Table 1 and Figure 12 were modelled with the JONSWAP spectrum, and the peak enhancement factor was set to 2.4, following the practice recommended in DNV GL (2017). The influences from the wind and ocean currents were disregarded in the numerical simulations for two reasons: a general trend of calm sea states and a lack of reliable predictions for these two types of loadings.

4. Results

4.1. Comparison of the WEC motions
The horizontal and vertical motions of the WEC were extracted from the 3-hour numerical simulations for all the cases presented in Table 1, and the corresponding information from the measurements were collected and post-processed for the same dates and time spans. Figure 13 presents a spectral analysis of the WEC's motions in the heave direction based on the measurement data and the results from the numerical simulations. Three examples of results from Table 1 are presented, which represent a case of longer T_p (June 16), a case of higher H_s (June 19), and a case near the resonant period of the WEC (June 18). The responses of the WEC's heave motions are essential to predict the power performance of the WEC, and hence, it is of interest for comparison. Satisfactory agreements were found in terms of the overall trends and the peak values of the spectra. The measurements show a somewhat broader-band spectrum than the simulations. Two peaks can be observed in

Table 1. Stationary time periods and sea states identified using the measured WEC motions.

| Time periods: date and time span	Estimation using the WEC motions			Prediction from the CMEMS data		
	H_s [m]	T_p [s]	θ [°]	H_s [m]	T_p [s]	θ [°]
2017–06–13 18:00:00–21:00:00	0.75	7.50	30	N/A	N/A	N/A
2017–06–14 02:00:00–05:00:00	0.60	7.50	60	0.86	7.87	324
2017–06–15 08:00:00–11:00:00	0.70	7.50	60	0.86	12.17	340
2017–06–16 10:00:00–13:00:00	0.95	10.00	30	1.16	12.04	344
2017–06–17 04:00:00–07:00:00	0.95	9.00	60	1.30	11.76	340
2017–06–18 08:00:00–11:00:00	1.40	6.75	30	1.69	6.81	8
2017–06–19 15:00:00–18:00:00	1.75	7.50	30	1.85	9.04	349
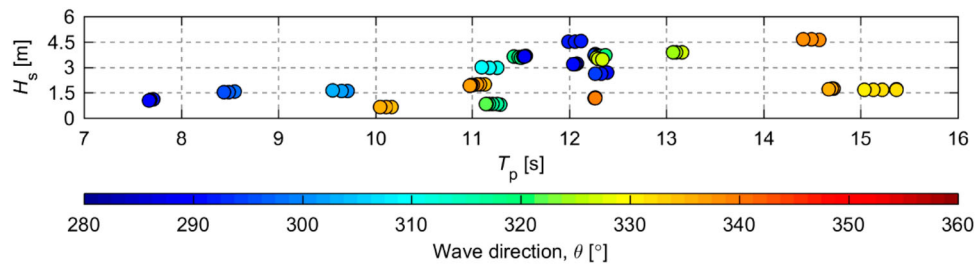
Figure 12. Prediction of the stationary wave load conditions using the CMEMS data.

the measurement data, while the simulations show only one. One reason for these differences was attributed to the initial assumption made to define a stationary sea state. It was assumed that each sea state is stationary for three hours and that the waves follow the JONSWAP spectrum with a fixed peak enhancement factor (see Section 3.2). This assumption may have been violated because in reality, it is likely that a sea state is stationary for a shorter time span and the wave spectrum at the test site should be represented by another model. Another reason specific for this study is that the test site and installation of the WEC is very close to an island, which may have affected the response spectrum.

Heatmaps were used to generate a visual representation of the area the WEC was operating within for the different sea states (see Figure 14). The red dots represent the initial position of the WEC system: for the 'simulation', the point is the origin of the numerical model, which is defined at the centre of the waterplane of the WEC buoy under still water conditions, and for the 'measurement', the point is defined as the average position based on all of the measurement data (e.g. all measurement data during 15:00:00 on June 13–22:00:00 on June 19). Thus, the heatmaps show the offset of the WEC from its 'expected' average location caused by the sea states presented in Table 1.

The largest distance from the average position (the red dot) is similar between the numerical simulation and the measurements; this aligns with the observations in Figure 13, which show that the simulations accurately predict the WEC's maximum movement. However, the results in Figure 14(a) show that the horizontal motions in the measurements are more scattered than those in the numerical simulations. The reason is that the numerical model assumes the same θ value throughout each 3-hour period, while the exact θ in the measurements may vary. In addition, the slightly larger ranges of vertical motion are observed in the measurements (see Figure 14(b)). Two plausible reasons for this observation were identified: the sea

state was close to but not fully stationary during the measurements (partly calmer in the simulations) and the tide affected the measurements. The latter cannot be modelled in the software, i.e. the water depth cannot be adjusted during an ongoing simulation. However, the influence of the tide was minor and assumed to not influence the mooring line forces to a large extent. In conclusion, the simulations and measurements were in good agreement.

4.2. Comparison of the mooring line forces

The location of the pressure sensors on the bollard structure corresponds to the fairlead point in the numerical simulation model. Thus, 3-hour time histories of the axial forces in the mooring line elements near the fairlead points were extracted for statistical analysis. Figure 15 presents the results of the measured and simulated mooring forces for Moorings 1 and 2 during the 7 periods presented in Table 1. Each dot represents the mean value of the mooring line force during a simulation, and the different lines represent the mean values and standard deviations from the measurements. During the post-processing of the measurement data, however, inadequate measurement accuracy of the load cells was observed in view of the calm sea states during most of the measurement period. It was decided to compare only the mean mooring line forces in this investigation because other statistical properties will not be reliable under these circumstances.

The results from the numerical simulations and the full-scale measurements show relatively good agreement. The mean values from the numerical simulations are on average 10% higher than the full-scale measurement results in both mooring lines. Note that even though the ocean current and wind loads were low during the measurement days and were not considered in the numerical model, they may have affected the full-scale measurements and slightly influenced the axial forces in the mooring lines. The numerical simulations reliably
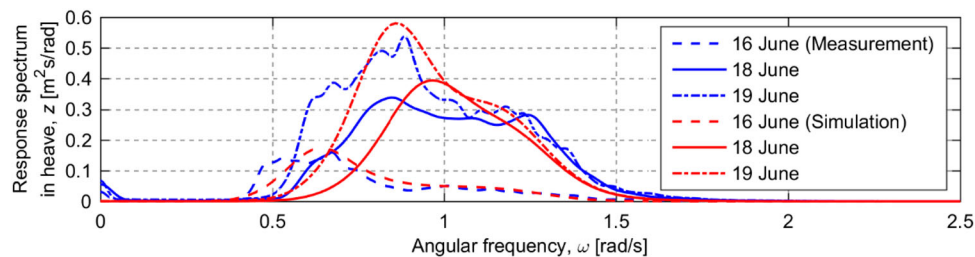

Figure 13. Response spectra for the heave motions of the WEC from the measurement data and numerical simulations.
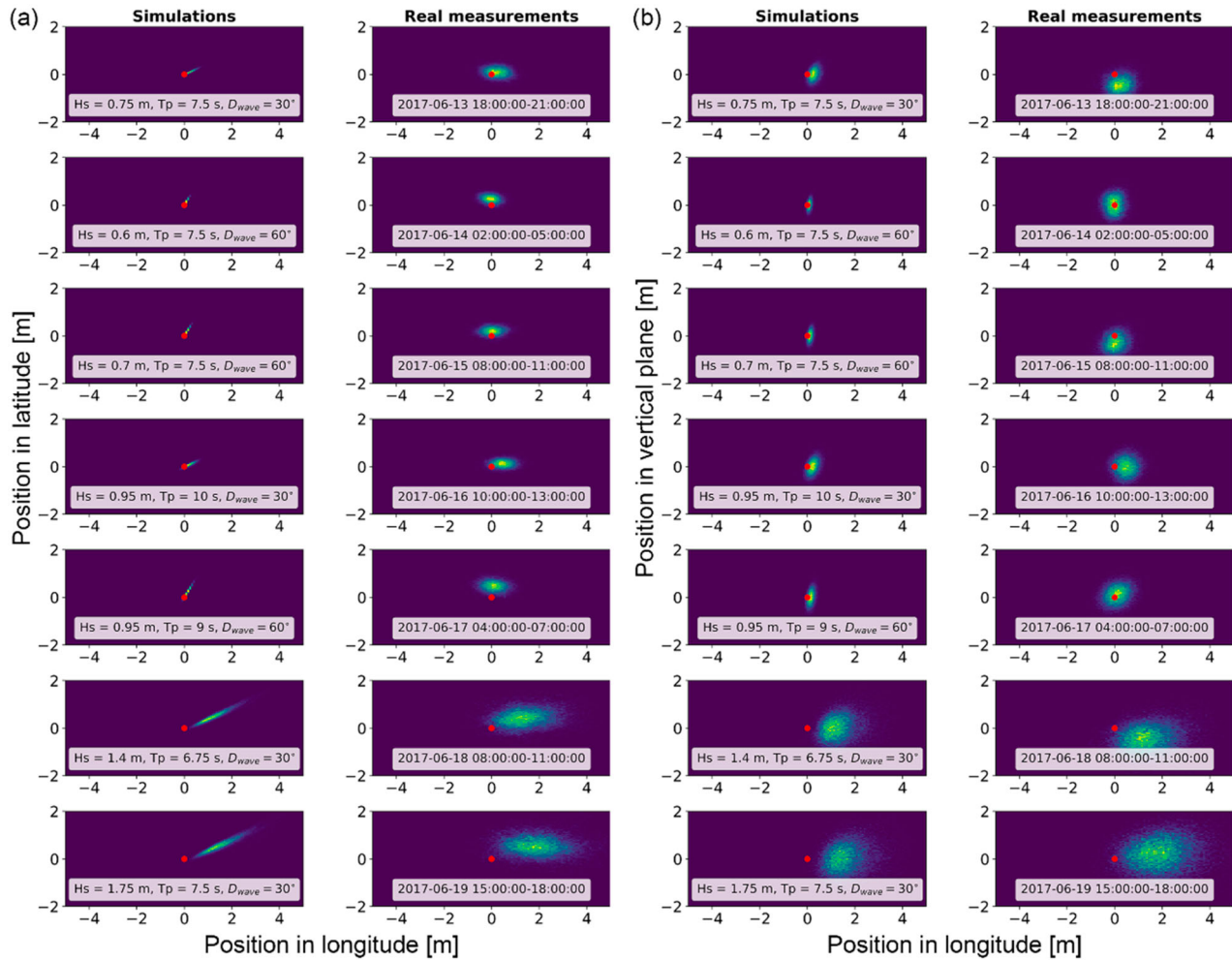
Figure 14. Heatmap of the WEC's motions in the (a) horizontal and (b) vertical planes. Each sub-figure shows results from the simulations (left) and measurements (right). The red dot represents the initial position of the WEC system.

captured the major trends that were also observed in the measurement data. First, Mooring 1 has higher axial forces than Mooring 2 since the former is more aligned with the incident wave load direction. Second, the force in Mooring 1 was higher on June 18 and 19 than on the earlier dates due to the change in the sea state conditions, and the force in Mooring 2 simultaneously decreased as a result of Mooring 1 carrying greater loads in the incident load directions.

Figure 16 presents a comparison of the mooring forces for all the stationary periods identified using either the WEC motion or the CMEMS data. The ratios of the simulated and measured mooring forces are 1.23 for Mooring 1 and 1.38 for Mooring 2. However, note that there are three periods that show substantially larger discrepancies. The reasons for these discrepancies were attributed to the model limitations in conjunction with the loading uncertainty. First, as discussed in Yang et al. (2018b), the power take-off (PTO) system of the WEC was numerically modelled as a linear damper with a primary focus on predicting the system's response under moderate sea states; the numerical simulations usually overpredict the motion and force responses under higher sea states. The three discrepancies all occurred in higher sea states; hence, the overprediction from the numerical simulation was expected. Second, there

are inherent uncertainties in the CMEMS data being used at the test site (see Section 3.2). Together, the existence of a few cases with larger differences were deemed acceptable. If these few cases were excluded from the comparison, the calculated ratios between the simulated and measured forces dropped to 1.11 for Mooring 1 and 1.15 for Mooring 2. Overall, it was again concluded that the prediction capacity of the numerical model is good with regard to the mooring forces.

4.3. Mooring line forces matrix

The motion of the WEC shown in Figure 11 revealed that the prevailing sea states might not be stationary for a complete 3-hour period. Figure 17 presents a summary of the calculated wave conditions based on the WEC motion measurements, wherein the stationary period was identified on a one-hour basis. Noticeable scatter in the sea state conditions during a day indicates the potential variations in the load conditions imparted on the WEC.

Figure 18 presents the mean force values in Moorings 1 and 2 corresponding to all the wave conditions shown in Figure 17; both measurement and simulation results are shown for comparison. For the measurements, it was assumed that the wave
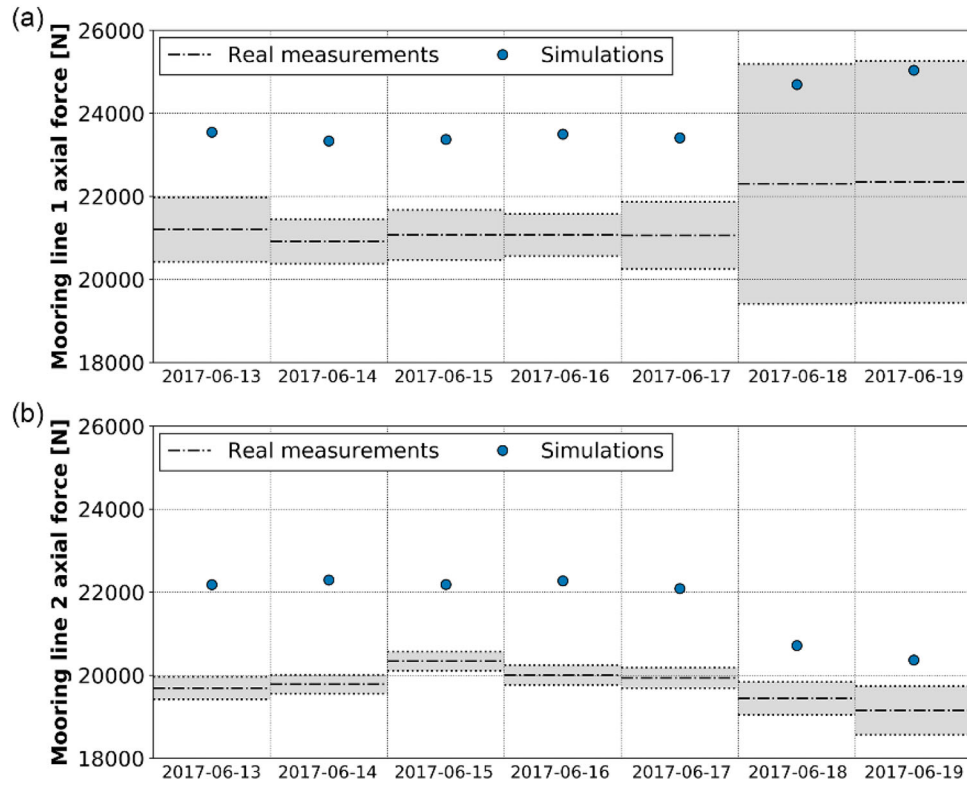
Figure 15. Axial forces in (a) Mooring 1 and (b) Mooring 2. A dot represents the mean value from a simulation, and the lines show the corresponding results from the measurements: dashed-dotted line (mean value) and dotted line (standard deviation).

conditions within a rectangle define a sea state. For example, the highlighted orange area in Figure 17 corresponds to a sea state with an H_s of approximately 1.75–2.00 m and a T_p of approximately 6–7 s irrespective of θ. Hence, the measured axial forces in the moorings could be calculated for each sea state as follows: the mean force value of a mooring line was calculated for every data point in a sea state; thereafter, the average value of the mean values was calculated to obtain the final mooring axial force results for the sea state under consideration. The simulation results were generated by performing a one-hour simulation for each sea state. The sea state for the same highlighted orange area in Figure 17 is then defined by

$H_s = 1.875$ m and $T_p = 6.5$ s (namely, the mid-values of the boundary values of H_s and T_p for each rectangle); θ was defined as 30° because of the observed high probability of occurrence based on the WEC motion measurements.

All observations made in Figure 16 remained valid for these two one-hour force matrices. In addition, an improvement in the prediction capability of the numerical model was observed. On a one-hour basis, the simulated mooring forces were on average 11% and 8% higher than the measured forces in Mooring 1 and Mooring 2; both are considerably lower than the values estimated on a three-hour basis (see discussion related to Figure 16)
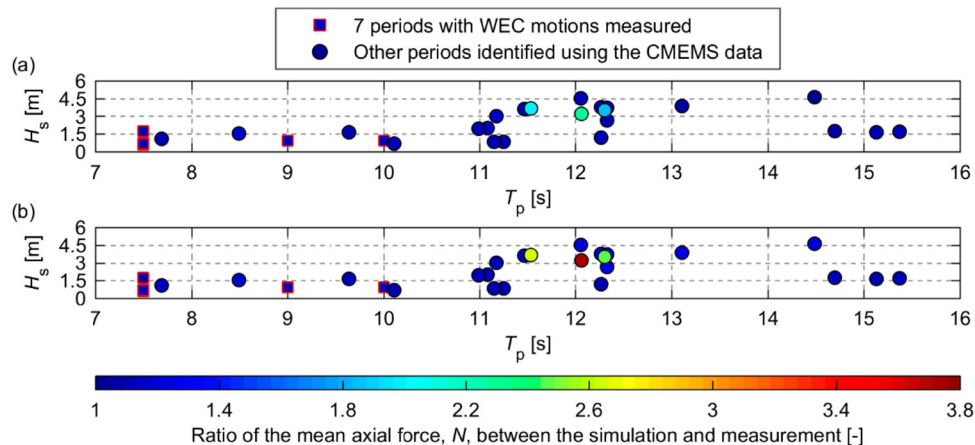

Figure 16. Comparison of the estimated mean forces of (a) Mooring 1 and (b) Mooring 2 under different sea states. All values are shown as the ratios between the simulated and measured values.
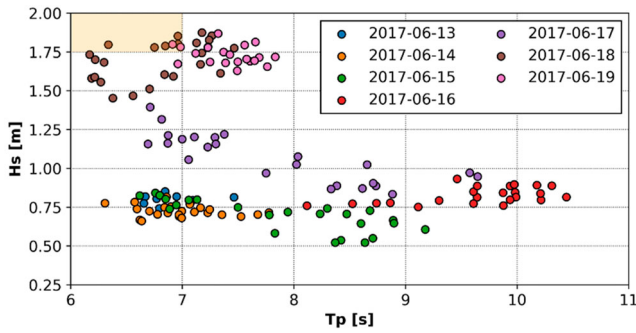
Figure 17. Summary of 1-hour wave conditions calculated based on the WEC motion measurements.

Note, however, that the results in Figure 18 fall primarily in the region of moderate/calm sea states. In Figure 19, the comparisons between the simulations and measurements were performed for all the available measurement data; hence, the prediction capability of the numerical model can also be examined for higher sea states. Overall, on a one-hour basis, the

simulations showed approximately 12% higher mean forces than the measured forces. The results in Figures 18 and 19 together indicate that changes in the sea state at the test site may generally occur during a shorter time span; it is thus recommended to compare the simulation against measurements on a one-hour basis for this study.

5. Discussion on the sources of uncertainties

The comparison of results from the full-scale measurements and the numerical simulation model of WaveEL 3.0 showed good agreement. However, some of the assumptions made in the simulation model pertaining to the analyses of the WEC motions and environmental loads need further investigation.

The sensors mounted on the WEC did not correctly measure the yaw angle. The method used to recover the yaw angle does not give a sufficiently accurate approximation of the yaw angle and contributes to uncertainty in the calculation of the WEC's motions and the sea states it was subjected to.
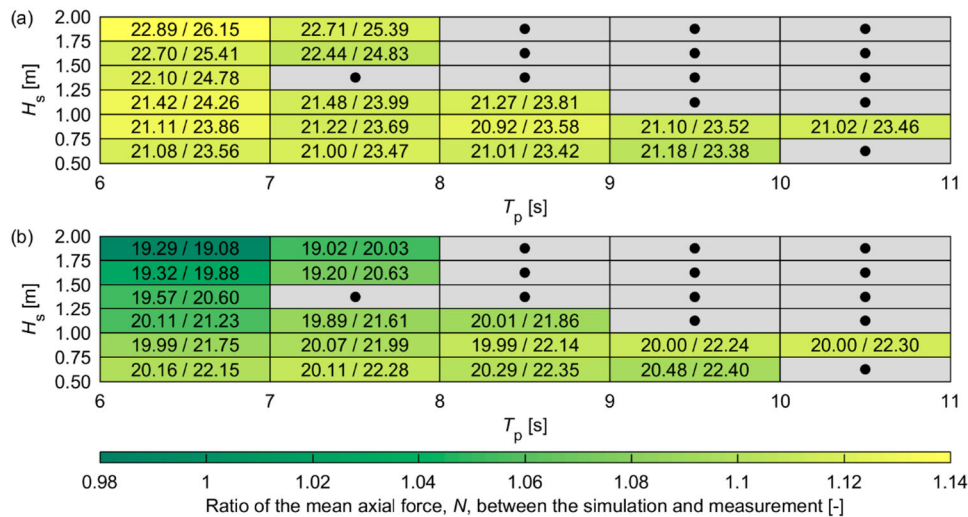

Figure 18. Axial force matrices for (a) Mooring 1 and (b) Mooring 2: average of all mean values. The two values shown in each coloured cell correspond to measurement and simulation results in kN.
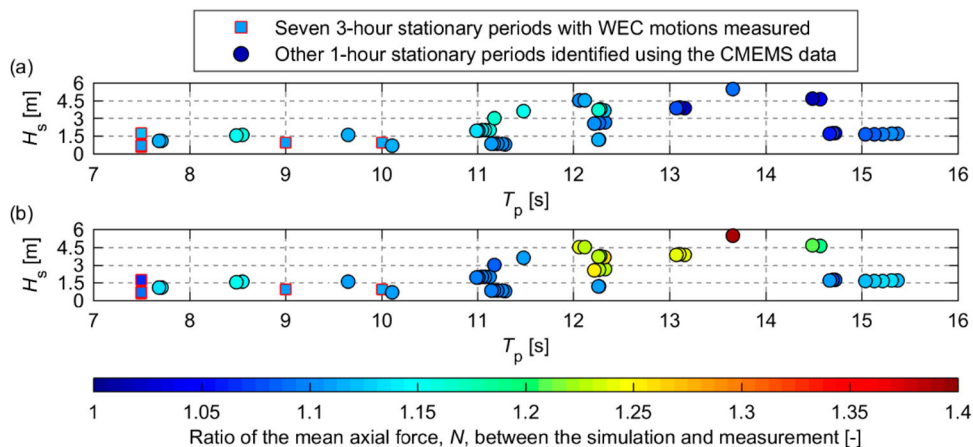

Figure 19. Comparison of the estimated mean forces of (a) Mooring 1 and (b) Mooring 2 under different sea states. Each point represents a 1-hour sea state. All other comparison criteria are the same as those for Figure 16.

The WEC's measured heave motions showed that there was some influence from the tide on the results (see Figure 11). It is not possible to change the water depth during an ongoing simulation in the software used in the study, and this effect was also assumed to be minor. A parameter sensitivity analysis should be performed in future work for different water depths to investigate how much the axial force in the mooring lines is influenced by the tide.

Without the WEC motion measurements as an input for the load identification, the agreement between the simulated and measured mooring forces was found to be less satisfactory; one plausible cause was the uncertainty of the wave direction predicted by the CMEMS data. During the six days where the WEC motion was measured, the potential loading direction was always found in the range between 0 and 60°; this aligns with the results in Eugster (2010), where it was observed that the prevailing wind is from the southwest at the test site. However, the dominant wave direction predicted by the CMEMS data was from the northwest. Provided that the CMEMS is based on the wave model for simulating open water, it is possible that the exact loading direction at the test site is different from the prediction from the CMEMS data. Yang et al. (2018a, 2018b) showed that the WEC motions and mooring force responses were highly dependent on the directionality of the load. Therefore, the less agreeable results observed in the cases where the loading directions were more uncertain was deemed reasonable.

The incident wave loads in the numerical simulations were assumed to be constant during each simulated case. Figure 14 shows that this is not the case in the measurements. Moreover, Figure 13 shows that the wave spectrum may have two peaks instead of one, which was assumed in this study. Further investigation is needed to quantify the sensitivity of the system's responses in relation to the wave realizations with regard to factors such as the wave spreading function and wave spectrum.

Wind and ocean currents, which may be present at the Runde test site, were excluded in this study. This assumption was justified because of the calm seas during most of the identified periods. The impact of excluding the wind and ocean currents is expected to be higher as the sea states become more severe; this rationalised the larger differences between the simulated and recorded mooring forces observed in Figures 16 and 19. A few initial simulations were performed to investigate the sensitivity of the WaveEL 3.0 system to wind and ocean current. No correlations among the waves, winds, and ocean currents were considered; the purpose of these simulations was simply to quantify the degree of sensitivity. The simulation results showed that the mean value of axial force can be increased by 30–60% in the mooring at the head-sea position, whereas the mean forces are decreased by 15–30% for other moorings due to the presence of the wave and current loads. Measurements of the wind and ocean currents can potentially be included in future investigations to reduce this source of uncertainty.

The mean values of the axial forces in the mooring lines were generally higher in the simulations than in the measurements. This observation may also be a result of the load cells being mounted on the WEC. It is uncertain how their calibration was performed. Furthermore, the mooring material properties were provided by the mooring design company, but there was no information available for their force-displacement curves during dry and soaked conditions for the exact moorings that were installed in WaveEL 3.0 in Runde.

The PTO system in the installed WEC in Runde and the simulation model of the installation are different (see Yang (2018) for the assumptions, definitions, and limitations of the PTO model). The numerical simulation model has a simplified PTO system, which explains why there are some differences in the WEC's vertical motions. This also influences the RAOs of the numerical model versus the RAOs of the installed WEC. This discrepancy contributes to an uncertainty in the method used to determine the stationary sea states. Further research is needed to analyse the magnitude of this uncertainty.

6. Conclusions

This study presented results from a measurement campaign where the recorded motions and axial forces in the mooring lines of Waves4Power's WEC system WaveEL 3.0 were compared with results from numerical simulations using a numerical model of WaveEL 3.0. Because of the lack of measured data of the sea state conditions at the test site, a method was proposed to construct the sea state conditions WaveEL 3.0 was subjected to by using the recorded data and RAO calculations.

The measured and simulated WEC's motion responses were found to be in good agreement. This shows that the methodology used to define the environmental loads (i.e. sea states) was sufficient for the purpose of this study. The methodology may be used at other test sites, but more verifications are needed before its general applicability can be confirmed. Furthermore, the measured and simulated axial forces in the mooring lines were also in good agreement. The numerical simulation results were mostly 10% higher than the measurements, which was within an acceptable range of error due to all uncertainties in the system instrumentation and environmental conditions. Therefore, the predictability of the numerical simulation model of WaveEL 3.0 is good.

A number of sources of uncertainties were discussed as well as their potential relevance for further study. Representation and modelling of the environmental loads (e.g. wave, wind, ocean current, incident load direction) in a numerical model is always related to large uncertainty and substantially influence the response of the system. Hence, these must be well motivated and preferably measured. In the design of new elastic mooring systems, the material properties of the mooring lines must be available for both dry and soaked conditions to correctly calculate the hydrodynamic and structural responses.

ORCID

Jonas W. Ringsberg ⓘ http://orcid.org/0000-0001-6950-1864

References

Banfield SJ, Flory JF, Hearle JW, Overington MS. 1999. Comparison of fatigue data for polyester and wire ropes relevant to deepwater moorings. Proceedings of the 18th International Conference on Offshore Mechanics and Arctic Engineering; Jul 11–16; Newfoundland, Canada.

CMEMS. 2017 Jun–Nov. Data from: Atlantic - European north west shelf - ocean wave analysis and forecast [dataset]. Copernicus Marine Environment Monitoring Service (CMEMS). [accessed 2019 Nov 24]. http://marine.copernicus.eu.

DNV GL. 2017. Recommended practice DNVGL-RP-C205 environmental conditions and environmental loads. Høvik, Norway: DNV GL AS.

DNV GL. 2019. SESAM software products overview. DNV GL AS. [accessed 2019 Nov 24]. https://www.dnvgl.com/software/products/sesam-products.html.

Eugster A. 2010. Runde meteorological station: data report for 2005–2009. Runde, Norway: Runde miljøsenter.

Kosleck S. 2014. Real-time-forecast of wave-structure interaction in natural sea states: Influence of the wave encounter angle. Proceedings of the ASME 2014 33rd International Conference on Ocean, Offshore and Arctic Engineering; Jun 8–13; San Francisco, California, USA.

Lang X, Yang S-H, Ringsberg JW, Johnson E, Guedes Soares C, Rahm M. 2018. Comparison between full-scale measurements and numerical simulations of mooring forces in a floating point-absorbing WEC system. Advances in Renewable Energies Offshore. Proceedings of the 3rd International Conference on Renewable Energies Offshore (RENEW 2018); Oct 8–10; Lisbon, Portugal, London: Taylor & Francis Group.

The MathWorks, Inc. 2016. MATLAB. Version R2016b. Natick (MA): The MathWorks Inc.

Runde Environmental Centre. 2018. Wave forecasting model at Runde by SWAN model. [accessed 2019 Nov 24]. http://swan.rundecentre.no/animations/.

Saulter A. 2017. Quality information document—North West European Shelf Production Centre. [accessed 2019 Nov 24]. http://cmems-resources.cls.fr/documents/QUID/CMEMS-NWS-QUID-004-012.pdf.

SINTEF Ocean. 2018a. RIFLEX. Version V4.10-03. Trondheim, Norway: SINTEF Ocean.

SINTEF Ocean. 2018b. SIMO. Version V4.10-03. Trondheim, Norway: SINTEF Ocean.

WAFO Group. 2017. WAFO. Version 2.5. Lund. Sweden: Lund University. http://www.maths.lth.se/matstat/wafo/.

Waves4Power. 2019. Installation of the WaveEL buoy on site at Runde. Gothenburg: Waves4Power. [accessed 2019 Nov 24]. http://www.waves4power.com/uncategorized/installation-of-the-waveel-buoy-on-site-at-runde/.

Yang S-H. 2018. Analysis of fatigue characteristics of mooring lines and power cables for floating wave energy converters [dissertation]. Gothenburg, Sweden: Chalmers University of Technology. doi:10.13140/RG.2.2.28560.66562.

Yang S-H, Ringsberg JW, Johnson E. 2018a. Parametric study of the dynamic motions and mechanical characteristics of power cables for wave energy converters. J Mar Sci Technol. 23(1):10–29.

Yang S-H, Ringsberg JW, Johnson E, Hu Z, Bergdahl L, Duan F. 2018b. Experimental and numerical investigation of a taut-moored wave energy converter: a validation of simulated buoy motions. Proc Inst Mech Eng M: J Eng Mar Env. 232(1):97–115.

Yang S-H, Ringsberg JW, Johnson E, Hu Z, Palm J. 2016. A comparison of coupled and de-coupled simulation procedures for the fatigue analysis of wave energy converter mooring lines. Ocean Eng. 117:332–345.

Yang S-H, Ringsberg JW, Johnson E, Hu Z. 2019. Experimental and numerical investigation of a taut-moored wave energy converter: a validation of simulated mooring line forces. Proceedings of the International Conference on Ships and Offshore Structures (ICSOS 2019); Sep 4–8, Melbourne, Florida, USA.